Nanoscale TEM Imaging of Hydrogel Network Architecture

Ryuji Kiyama, Masahiro Yoshida, Takayuki Nonoyama, Tomáš Sedlačík, Hiroshi Jinnai, Takayuki Kurokawa, Tasuku Nakajima, and Jian Ping Gong**

Dr. R. Kiyama, Prof. T. Nonoyama, Dr. T. Sedlačík, Prof. T. Kurokawa, Prof. T. Nakajima, Prof. J. P. Gong, Faculty of Advanced Life Science, Hokkaido University, Sapporo 001-0021, Japan

Mr. M. Yoshida, Graduate School of Life Science, Hokkaido University, Sapporo 001-0021, Japan

Prof. T. Nonoyama, Dr. T. Sedlačík, Prof. T. Kurokawa, Prof. T. Nakajima, Prof. J. P. Gong, Global Station for Soft Matter, Global Institution for Collaborative Research and Education (GI-CoRE), Hokkaido University, Sapporo 001-0021, Japan

Prof. H Jinnai, Institute of Multidisciplinary Research for Advanced Materials, Tohoku University, Sendai 980-8577, Japan

Prof. T. Nakajima, Prof. J. P. Gong, Institute for Chemical Reaction Design and Discovery (WPI-ICReDD), Hokkaido University, Sapporo, 001-0021, Japan
Tel: +81-11-706-9011; E-mail: nonoyama@sci.hokudai.ac.jp
Tel: +81-11-706-9011; E-mail: gong@sci.hokudai.ac.jp

Keywords: Hydrogel, Polymer network, Direct observation, Transmission electron microscopy, Double Network, Mineral staining, Inhomogeneity, Dangling chain

In this work, we succeeded in direct visualization of the network structure of synthetic hydrogels with TEM by developing a novel staining and network fixation method. Such a direct visualization had not been carried out because sample preparation and obtaining sufficient contrast are challenging for these soft materials. TEM images revealed robust heterogeneous network architectures at mesh size scale and defects at micro-scale. TEM images also revealed the presence of abundant dangling chains on the surface of the hydrogel network. The real space structural information provides a comprehensive perspective that links bulk properties with a nanoscale network structure, including fracture, adhesion, sliding friction, and lubrication. The presented method has the potential to advance the field.

1. Introduction

Hydrogels are important soft materials with broad applications in society, especially as biomaterials, stretchable electronics, etc[1–4]. A typical hydrogel is a crosslinked hydrophilic polymer that shows rubber elasticity and does not dissolve in water. As a feature of soft matter, the structure of the hydrogel network does not have long-range order and is heterogeneous at various scale levels. Typically, at the nanoscale, the polymer chains between crosslinking points have distribution in molecular weight along with loops and dangling chains[5]; at the microscale, large voids and defects induced during coagulation of microgels to bulk gels often exist[6–8]. The physical properties of a hydrogel strongly depend on the architecture of the polymer at different scales. For example, loops and dangling chains contribute to solvation and thereby swelling ability as like network chains but do not contribute to the elasticity of a hydrogel; the network mesh size regulates the molecular diffusion and transportation; the largest defect in the hydrogel formed during preparation process governs the fracture strength of the material[9]. Observing the structure of network materials from the nanoscale network level to the microscale level is of paramount importance for understanding and predicting the physical properties and rational design of this class of materials.

As the state-of-the-art approach, the X-ray/neutron/light scattering are powerful methods to characterize the physical structure of hydrogels at different length scales from

58 nano to micro[7,10,11]. However, the scattering methods give average structural information
59 over a scattering volume several orders of magnitude larger than the mesh size of the network
60 (typically 10 ~100 nm). Moreover, explaining the scattering results in reciprocal space is
61 usually difficult without complementary real space structure information.
62 Transmission electron microscopy (TEM) is one of the most promising methods to
63 directly image material structures with nanoscale resolution in real space. Recent progress in
64 tomography TEM technology clarifies the three-dimensional structure of polymer materials at
65 the nanoscale[12]. However, applying TEM to observe the network structure of hydrogels that
66 consist of thin, flexible polymer chains swollen in water is highly challenging. Existing TEM
67 observation methods, such as electron staining, phase contrast, and scanning TEM, are
68 difficult to give sufficient electron density contrast for individual polymer chains of synthetic
69 hydrogels[13–16]. Resin substitution or cryogenic environment (Cryo-TEM), required to
70 suppress the thermal fluctuation of the soft materials[17,18], will provide a similar electron
71 density between the thin polymer strands of a hydrogel network and the surrounding matrix,
72 resulting in no contrast. The difficulty is to develop a method that can selectively stain the
73 thin target polymer strand to produce a sufficient electron density contrast and spatial
74 resolution while maintaining the polymer network architecture. The extremely soft and thin
75 synthetic polymers undergo large deformation during staining or dehydration compared to
76 relatively rigid and thick polymers like DNA[19,20].

77 Here, we developed a method to prepare hydrogel specimens for TEM observation.
78 This method allows for performing selective staining, dehydration, and resin substitution
79 without causing fatal changes in network architecture. With this method, for the first time, we
80 succeeded in observing the network architecture of chemically crosslinked, vinyl-type
81 polyelectrolyte hydrogels in real space over a wide length scale, from the network architecture
82 in tens nm to meso-scale heterogeneity in μm. For the first time, we also succeeded in
83 visualizing the existence of graft chains on the surface of the network. These observations
84 provide important insights for understanding the kinetics of polymer network formation,
85 fracture behavior, and the surface properties of hydrogels. This TEM observation method has
86 the potential to be applied to other rubbery network materials with various chemical structures
87 and has the potential to advance the field.
88

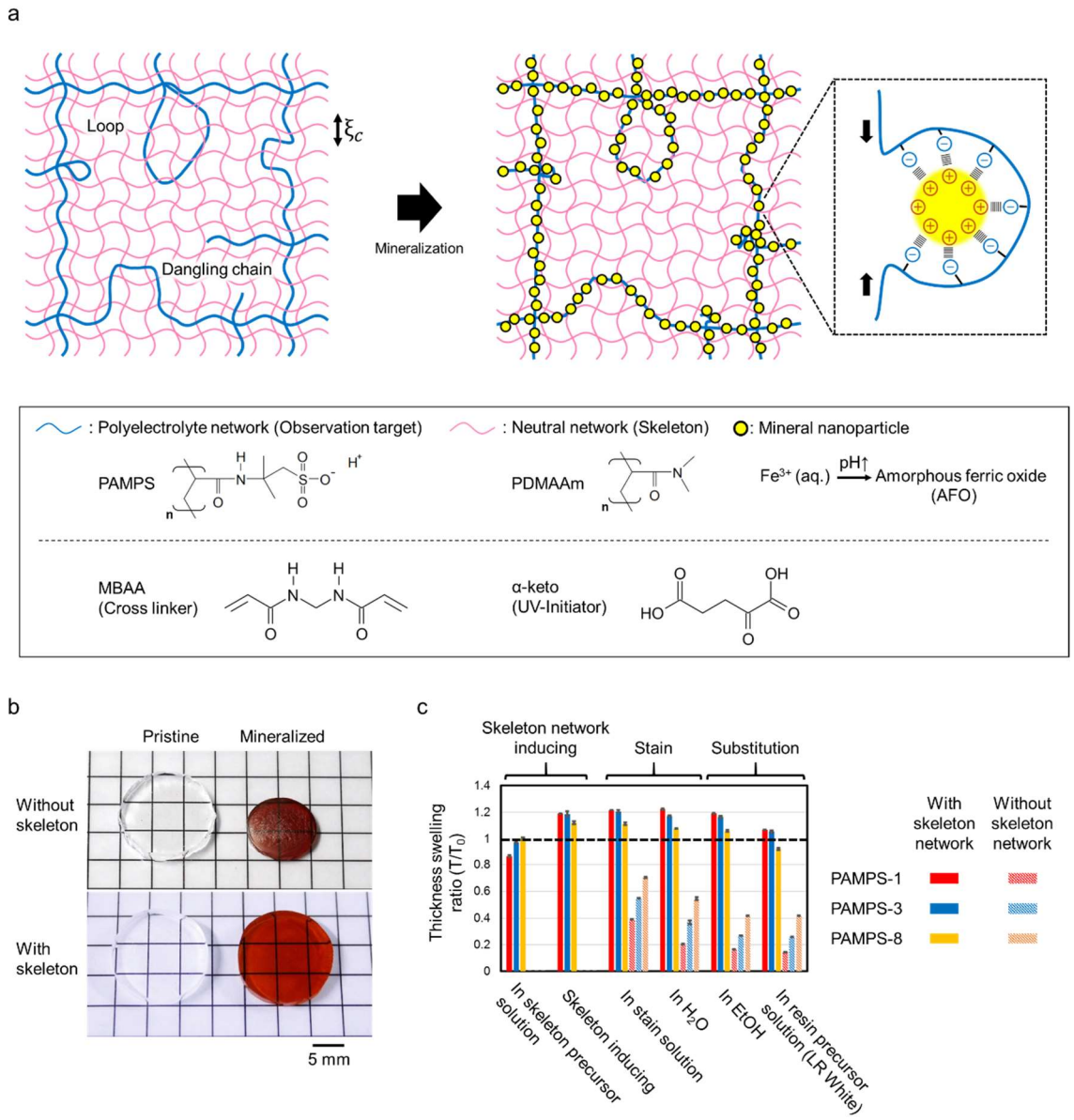

Figure 1. (**a**) Schematic illustration of the double-network method to stain a polyelectrolyte network at isovolumic condition for TEM observation. ξ_c is cut-off length for structure preservation. Crosslinking positions and strand conformation of the polymer network at large scale ($>\xi_c$) are preserved, while interaction between polyelectrolyte and mineral generates shrinking force, and the network strands collapse, loosing conformational information at small scale ($<\xi_c$). Conformational information of relatively short dangling chains is also not

preserved. (**b**) Appearance of the PAMPS-4 network gel with and without skeleton PDMAAm network before and after staining. (**c**) Thickness swelling ratio of the PAMPS networks with different crosslinker ratio during skeleton network inducing, staining, and resin substitution. Resin substitution is a process to replace the water in the hydrogels with solidified resin for TEM observation in vacuum (see details in Experimental section). Samples are coded as PAMPS-C_x, where C_x stands for the crosslinker ratio (mol% in relative to monomer). T_0 is the thickness of the PAMPS single network swelled in water. The black dashed line in the graph indicates the iso-volume line (T/T_0=1). By inducing the PDMAAm skeleton, the samples swell slightly (T/T_0=1.1-1.2). The samples without a skeleton network significantly shrink in staining solution and in resin precursor solution (T/T_0=0.1-0.4). With the skeleton network, the change in the final thickness of the resin-cured specimen is within 10% (T/T_0=0.9-1.1). The error bars indicate the standard deviation for five samples.

2. Results and Discussion

2.1. Strategy to staining target networks while reserving structure

The strategy is illustrated in **Figure 1a**. We chose a polyelectrolyte network carrying negative charges as our target network for two purposes. One reason for such selection is to pre-stretch the network strands into a highly extended state in favouring the network architecture observation. The counter-ions of a polyelectrolyte network exert a large osmotic

115 pressure to significantly swell the network in low ionic strength aqueous solution,
116 spontaneously achieving the highly pre-stretched state of the polymer strands. The other
117 reason is to selectively stain the target network by mineralization using metal ions. To hold
118 the polyelectrolyte network in the pre-stretched state during staining and the afterward resin
119 substitution process for TEM observation under vacuum condition, we introduce a neutral
120 polymer network of high concentration as a skeleton matrix before staining[21–23]. The neutral
121 polymer network, topologically interpenetrated with the target polyelectrolyte network,
122 generates a high osmotic pressure to prevent the shrinkage of the polyelectrolyte network in
123 the ionic staining solution[24]. The isovolumic staining preserves the crosslinking position and
124 mesh size of the target network and therefore allows us to clarify the architectural feature of
125 the target network. The conformation of the polyelectrolyte strands below a certain small
126 length scale is not preserved and changes upon staining. This cut-off length scale ξc below
127 which the strand conformation is not preserved should depend on the balance between the
128 energy gain by mineral staining and the elasticity penalty of both the target network and the
129 skeleton network. On the other hand, loops and undulating structures of chains larger than ξc
130 can be preserved because their deformation is inhibited by entanglement with the neutral
131 network.

132 Specifically, we adopted poly(2-acrylamido-2-methyl propanesulfonic acid)
133 (PAMPS) hydrogels synthesized by free radical polymerization as the target network. For the

134 skeleton network, we adopted poly(dimethylacrylamide) (PDMAAm) since we discovered
135 that among several neutral polymers tested, PDMAAm could maintain the isovolumic
136 condition of the target network not only during the mineral staining but also during the later
137 resin substituting process (see details in experimental section). We introduced the skeleton
138 network by synthesizing the PDMAAm network in the presence of the target PAMPS
139 network, using the double network technique [21–23]. To selectively stain the target
140 polyelectrolyte network with enough electron density contrast, we adopted Fe^{3+} that forms
141 amorphous ferric oxide (AFO) nanoparticles through heterogeneous nucleation on the
142 sulfonic acid groups of PAMPS chains [25]. In this study, we synthesized all hydrogels with a
143 commonly used crosslinker: N, N'-methylenebisacrylamide (MBAA) and UV initiator: 2-
144 oxoglutaric acid (α-keto).
145 The polymer volume fraction of the water-swollen PAMPS gels studied in this work
146 was 0.2 – 3.8 vol%, depending on the chemical crosslinker ratio relative to monomer in the
147 precursor solutions of PAMPS gels (see Experimental section). Direct staining of AFO on
148 water swollen PAMPS network caused substantial shrinkage of the gel (**Figure 1b**) and large
149 mineral formation **(Figure S1**), indicating the collapse of the network strands. The volume
150 shrinkage of the PAMPS network during AFO staining is suppressed in the presence of the
151 skeleton network PDMAAm, as confirmed by the small change in sample size (**Figure 1b**). In
152 these PAMPS hydrogels, the volume ratio of the skeleton network to the target PAMPS

153 network was 5 to 100, depending on the crosslinker ratio of PAMPS. We quantitatively
154 studied the volume changes of PAMPS hydrogels during the specimen preparation process by
155 characterizing the specimen thickness relative to that in pure water (**Figure 1c**). PDMAAm
156 can maintain approximately the same thickness of the specimen not only in staining solution
157 but also in ethanol and in the precursor solution of resin for substitution. As a result, the final
158 thickness change of PAMPS network relative to their water swollen state is less than 10% for
159 all PAMPS gel samples prepared with different formulations. This isovolumic condition
160 means the positions of the crosslinking points, and therefore the distribution of end-to-end
161 distances of the PAMPS network strands between crosslinking points (i.e., the mesh size), are
162 maintained in the TEM specimen.
163
164 **2.2. Nanoscale TEM observation of the networks**
165 To confirm that AFO is selectively mineralized on the PAMPS network but not on the
166 PDMAAm network, we first performed the TEM observation on the PAMPS microgels
167 embedded in the bulk PDMAAm gel[26]. **Figure S2** shows the optical microscopic image of
168 the PAMPS microgels, TEM images of PAMPS microgels in the PDMAAm gel, and their
169 corresponding schematic illustrations. The PAMPS microgels before mineralization (not
170 shown in the figure) are unseen by TEM, while spherical microgels with several micrometer
171 diameters are clearly identified after mineralization. This result indicates that AFO is

selectively stained on the PAMPS network but not on the PDMAAm network since the sulfonic group of PAMPS can catalyze the AFO deposition.

To observe the nanoscale PAMPS network structure, first, we adopted a porous PAMPS hydrogel containing large interconnected pores with ~10 μm gel walls[27]. The large pores provide a fast iron ions supply, thereby favoring sufficient mineral staining. The TEM micrograph shows the fine network architecture of the PAMPS **(Figure 2a)**. Under high magnification, it is clearly observed that AFO nanoparticles with a diameter of several nanometers are stained on the network with a mesh size of several tens of nanometers. The two-dimensional Fourier transform image of a single nanoparticle has no obvious peaks (lower right in **Figure 2a**), indicating its amorphous nature. Element mapping by using a scanning TEM further shows that the positions of sulphur of PAMPS and iron of AFO overlap on the nanoscale (**Figure 2b**), confirming that only the PAMPS network was selectively stained with ferric oxide. Furthermore, TEM tomography was performed to observe the 3D network structure **(Figure 2c and Supplementary Video**). 3D connection of the network consisting of four-arm crosslinking points is clearly observed. To the authors' knowledge, this is the first 3D nanoscale direct observation of network structure for soft synthetic polymers.

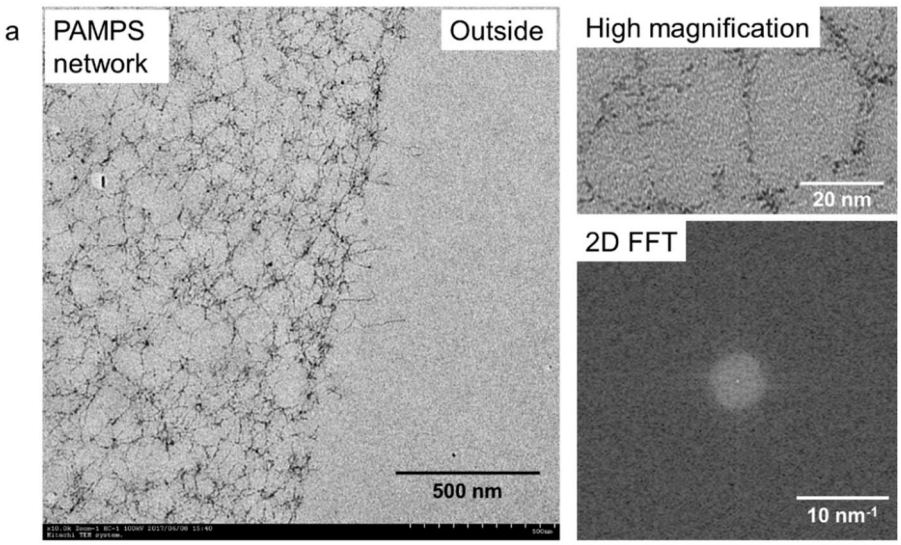

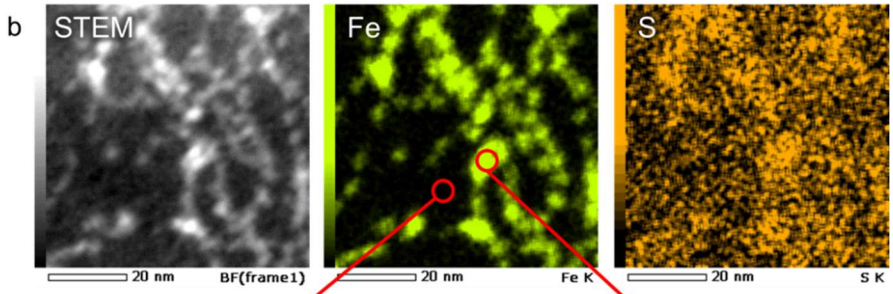

Element	wt%	σ
C	99.88	0.53
S	0.10	0.03
Fe	0.02	0.01

Element	wt%	σ
C	95.45	0.84
S	0.31	0.12
Fe	4.24	0.94

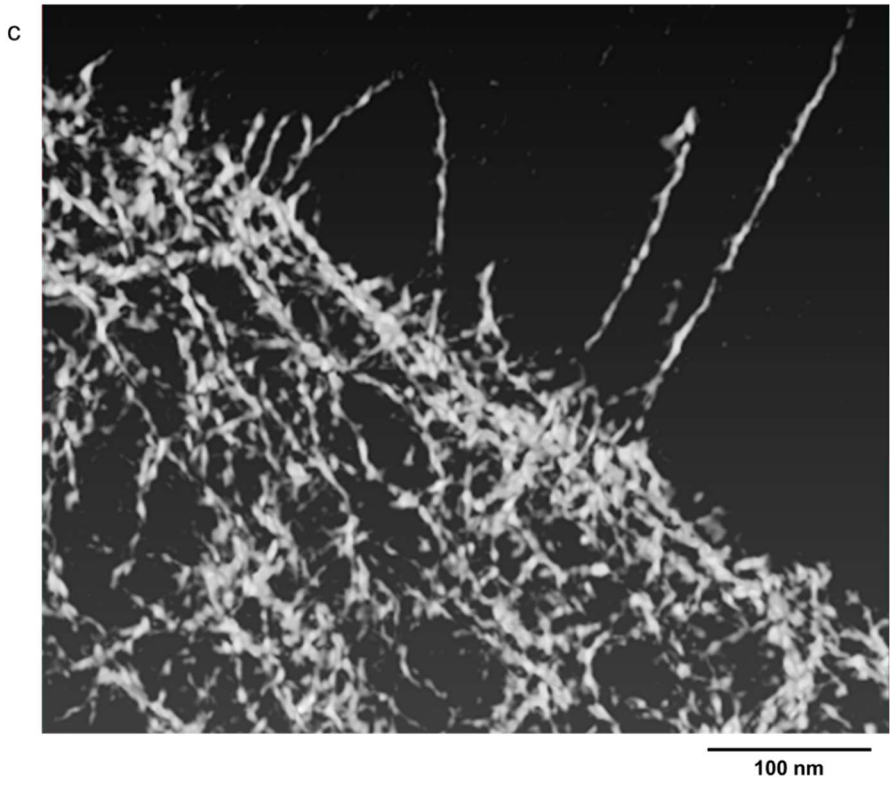

Figure 2. TEM observation of PAMPS network. (**a**) Low and high magnification TEM images and 2D FFT from a single mineral nanoparticle. (**b**) STEM elemental mapping. Fe and S shows the iron in the ferric oxide nanoparticles and sulphur in the PAMPS gel network, respectively. (**c**) TEM tomography image. A porous PAMPS gel with a wall thickness of approximately 10 μm was used for the observation. TEM sample thickness was about 100 nm

To understand the applicable range of this method, PAMPS hydrogels prepared with different crosslinker ratios were observed (**Figure 3 and S3**). There are two possible causes to make a large difference between the actual network structure and the TEM image: under-staining and inter-chain aggregation. When under-staining occurs, the mineral particles fail to adhere to the entire chain, resulting in a dots-like appearance in TEM images. This phenomenon occurred with too fine mesh gels (more than 3 mol% crosslinker, **Figure S3**), while the staining progressed sufficiently for large mesh gels (1 to 3 mol% crosslinker, **Figure 3**), and continuous network structures were observed. The under-staining is considered due to insufficient mineral supply. Higher concentration mineral source or longer reaction time may be the solution. When inter-chain aggregation occurs, multiple chains combined with a large mineral are formed, as shown in **Figure S1**, and the individual polymer structure collapses. In the PAMPS gels containing the skeletal network (**Figure 3b**), the formation of such huge minerals was inhibited, and there were only small minerals of uniform size, so it is considered

that inter-chain aggregation hardly occurred, and individual polymer structure was observed. Rarely, in areas where the mesh size is locally small, relatively large minerals of about 10 nm formed by interchain aggregation can be seen (**Figure 3b,** PAMPS-2 and PAMPS-3) because the distance between chains is close and the skeleton mesh cannot sufficiently inhibit aggregation. Such mineral particles may act as artificial cross-linking points, creating fake network structure, so caution is necessary. As a result, we concluded that in gels with a crosslinker concentration of 1 to 3 mol %, under-staining and inter-chain aggregation are negligible, and the network structure above the cut-off length remains almost unchanged in the TEM image.

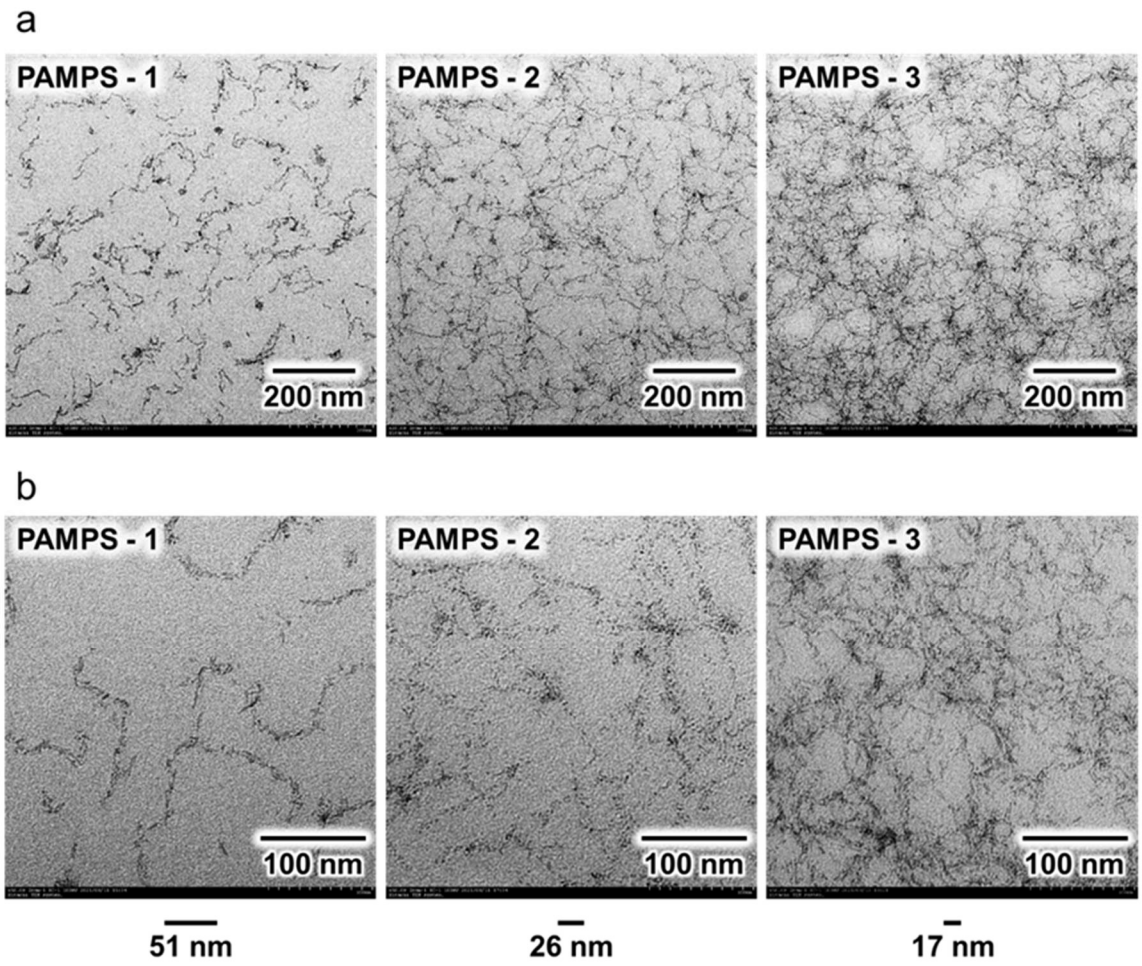

Figure 3. TEM images of the PAMPS networks prepared with different crosslinker ratio. (**a**) Low magnification images. (**b**) High magnification images. Samples are coded as PAMPS-C_x, where C_x stands for the crosslinker ratio (mol%). The mesh sizes calculated from PAMPS gel bulk modulus (**Table S1**) are shown by bars in the bottom. Since the specimen thickness is about 100 nm, the mesh with a size larger than 100 nm appears as unconnected.

Next, we discuss polymer conformation change on a small scale. TEM images reveal that the network strands have a persistent length of about 40 nm (**Figure S4**). This persistent length could be understood as the cut-off length ξ_c below which the initial conformation

information of the polymer strands is lost by mineralization. TEM images should represent unperturbed polymer strands conformation at a scale larger than this value. This is revealed by the winding structures (tens nm) between the cross-linking points in the PAMPS-1 sample that has a relatively long strand length among the three PAMPS networks (**Figure 3**). We notice that the cut-off length ξ_c is larger than the mesh size of the skeleton (8 ~ 10 nm) (**Table S2**). This could be understood by the low crosslinking ratio (0.1 mol%) of the skeleton network, which gives a relatively small elastic penalty for the collapse of the target strands by staining. During staining, partial collapse of the strands at a scale below ξ_c should exert additional tension on the target network. Since each crosslinking point is stretched from four different directions, the tension induced by shrinkage should be cancelled. As a result, the positions of crosslinking points should be preserved at a scale smaller than the cut-off length ξ_c. In fact, we can observe a network structure (about 20 nm mesh size) smaller than ξ_c in PAMPS-3 (**Fig.3**).

Based on the above discussion, we quantitatively confirmed whether the network structure was accurately observed by TEM. For that, we estimate the accumulative length of the polymer strands observed in the TEM image, using the PAMPS-1 sample as an example (**Figure S5a**). The high magnification TEM images of the PAMPS-1 are shown in **Figure S5b**. A fine PAMPS network morphology with a mesh size of a hundred nano-meter is observed. The discontinuity of the network can be attributed to the mesh structure that is

247 frequently larger than the thickness of the TEM specimen (100 nm). The accumulative strand
248 length in the volume of the TEM view (896×896×100 nm^3) is measured as L_{2D}=17700±2700
249 nm (see experimental part and **Figure S5a**). Since this length in the 2D TEM image is the
250 projection of length in 3D space, we correct it into 3D length by multiplying a factor of π/2 as
251 $L_{3D} = 2.8 \times 10^4$ nm (see experimental part). This is 21% of the total length of polymer 1.3×10^5
252 nm calculated from the amount of AMPS monomer unit in the viewing volume. Since the
253 polymer strands at a scale smaller than the cut-off length ξ_c are collapsed by staining, this
254 accumulative strand length should be corrected to get the true contour length of the single
255 polymer chain. A simple model derived a corrected factor of 1.4 for this effect (see
256 experimental part), which gives a value of approximately 30% of the total length of the
257 polymer. Accordingly, the TEM observation reproduced almost the 1/3 length of the network.
258 The remaining 70% monomers can be assigned for dangling chains and small loops which
259 cannot entangle with the skeleton, and they should take collapsed conformation and appear as
260 small dots in the TEM image. The large aggregations in **Figure S5b** indicated by black arrows
261 are ascribed to dangling chains on the network.

262 Furthermore, we qualitatively compare the mesh size in TEM images with that
263 calculated from Young's modulus of the bulk samples based on rubber elasticity theory [28]
264 (**Table S1**, **Figure 3b**). The increase of the crosslinker ratio results in the decrease in mesh
265 size in TEM images. The average mesh sizes calculated from the mechanical measurement at

266 the corresponding swelling state of TEM observation were shown by length bars under
267 corresponding TEM images in **Figure 3b**. These mechanically determined mesh sizes are in
268 the same order of magnitude with TEM images. Since the high-magnification TEM images
269 (**Figure 3b**) captured relatively sparse network density area for easy to observe, the network
270 sizes look larger than the calculated values, but as low-magnification images (**Figure 3a**)
271 indicate, hydrogel network is extremely inhomogeneous. Areas of high mesh density push
272 down the average mesh size and may carry more load. Considering that the accumulated
273 contour length of the polymer network in TEM is about 30% of the theoretical length, these
274 network structures observed in TEM are almost consistent with the prediction from
275 mechanical property and not a result of under-staining or inter-chain aggregation.
276
277 **2.3. Surface structure of network**
278 The surface feature, such as friction, adhesions, and permeability for small molecules
279 and ions, is an essential characteristics of network materials. Especially, hydrogels show
280 attractive surface nature, for example, in nature, hyaline cartilage exhibits both incredibly low
281 friction property and semi-permeability that allows nutrient diffusion[29,30]. Our TEM
282 observation for the first time revealed the precise structure of the polymer strands at the
283 chemically synthesized hydrogel network surface. When observing the bulk network
284 structure, we fixed the target network by physical entanglement with the skeleton network,

but dangling chains inside the network or on the surface cannot be fixed by this mechanism. Therefore, we adapt another strategy based on two previously established pieces of knowledge.

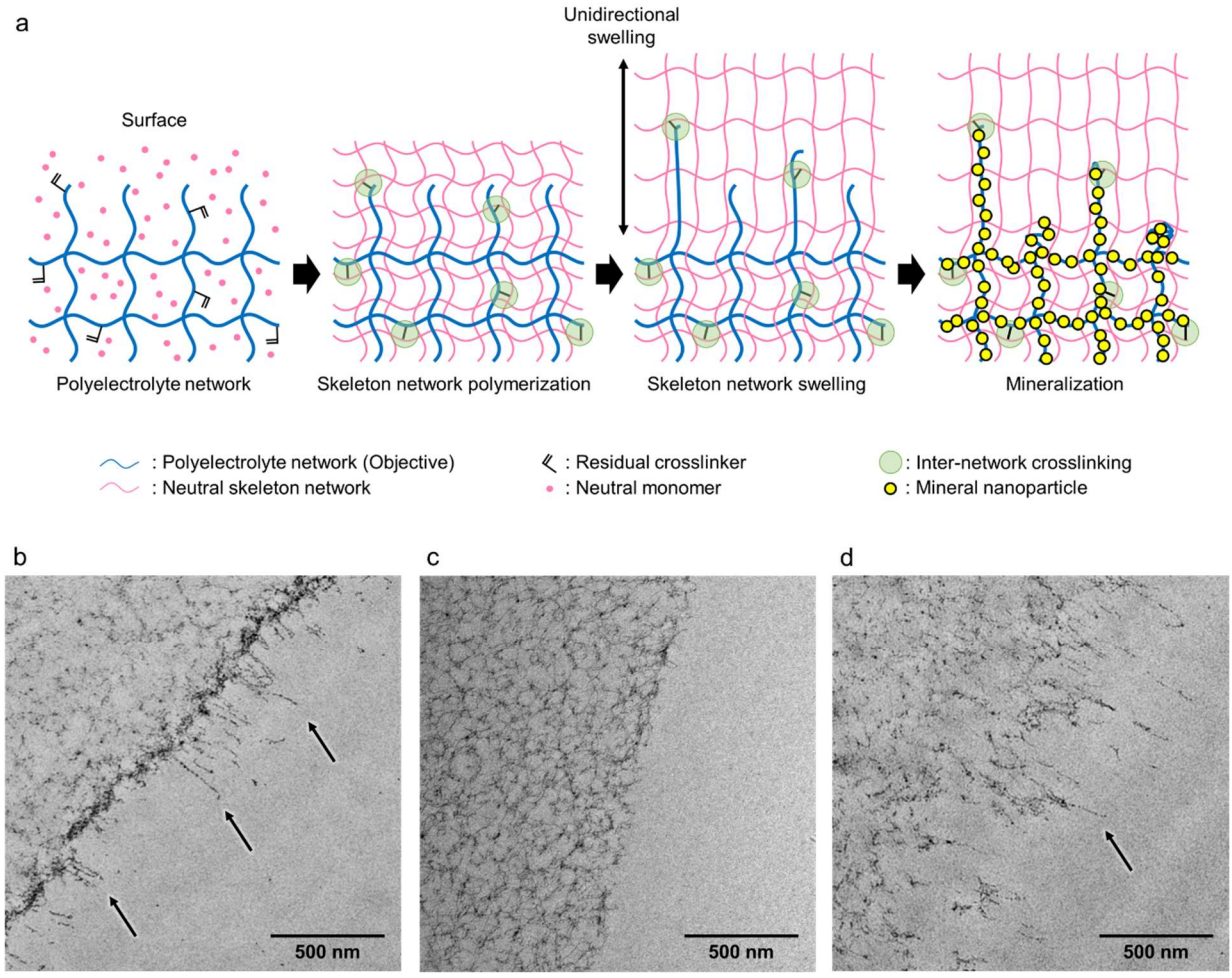

Figure 4. Surface network structure of the PAMPS gel. (**a**) Schematic of the surface dangling chain extension by the skeleton network. (**b, c**) Virgin PAMPS-4 network surface with (**b**) and without (**c**) inter-network crosslinking to the skeleton network. Before skeleton network polymerization, the residual crosslinkers in PAMPS network (**c**) were inactivated with the excess amount of initiators[31]. (**d**) Cut PAMPS-4 network surface with inter-network

crosslinking to the skeleton network. The PAMPS hydrogel was cut with a microtome knife and then was immersed in the precursor solution of the skeleton network to form PAMPS network embedded in skeleton matrix. The virgin surfaces in (**b**) and (**c**) were synthesized on a flat glass mould. The black arrows in the TEM images indicate surface dangling chains. The plain regions without network structure on the right part of the images (**b-d**) correspond to the skeleton network.

One is fixing the dangling chains to the skeleton network through the inter-network chemical crosslink[31]. As illustrated in **Figure 4a**, the PAMPS network usually contains a few unreacted vinyl groups after polymerization due to partial reaction of the crosslinkers. During the polymerization of the second skeleton network, some PAMPS dangling chains with residual vinyl groups are incorporated into the PDMAAm network. The other is inducing a layer of skeleton network on PAMPS surface during the skeleton network formation in PAMPS. When inducing the neutral skeleton network, a PAMPS network is sandwiched between glass plates. Counter-ion osmotic repulsion between the PAMPS and glass that are both negatively charged in water induces a layer of PDMAAm precursor solution at the interface. As a result, the PAMPS sample surface is covered by a layer of the neutral network of several micrometers-thick after polymerization of the skeleton network [32]. In fact, the neutral PDMAAm layer is clearly seen on the topmost surface of the specimen in a TEM

image at low magnification (**Fig. S6**). Therefore, the immersion of the PAMPS gel with the PDMAAm network in water induces the unidirectional swelling of the PDMAAm network surface layer towards the thickness direction since the already highly stretched PAMPS network confines the lateral direction. As a result, the PAMPS strands connected to the PDMAAm network are stretched in the direction vertical to the PAMPS network surface, and we can observe the approximate length of the PAMPS dangling chains.

Figure 4b shows the outermost as-prepared surface of a PAMPS-4 hydrogel synthesized on a flat glass mould. Dangling chains of several hundred nano-meter lengths (indicated by the black arrows) in a fully elongated state from the PAMPS network surface are observed. These dangling chain lengths are in the same order as network mesh size in the bulk region. Therefore, dangling chains can be assumed to be strands that could not find a crosslinking partner at one end. In addition, this result indicates that the length of the surface dangling chain of the chemically crosslinked network is comparable to the bulk network mesh size; thus, the length of the dangling chains of the gel surface can be estimated based on the mesh size of the bulk network. It should be noted that only dangling chains that have inter-network crosslinking with the neutral skeleton network are observed as elongated strands. Dangling chains not covalently connected to the skeleton network collapse into a globule conformation by staining. This is clearly seen by the dark rough line on the gel surface, similar to the dangling chains inside the gel (**Figure S5b**). In addition, no elongated dangling

chains were observed on the surface of the PAMPS network that had been treated with the excess amount of initiators to inactivate the residual crosslinkers by radicals (**Figure 4c**)[31].

We also observed the surface of the PAMPS gel cut using a fine microtome knife with an edge thickness of 76 μm. We synthesized the skeleton network after cutting the PAMPS gel so that some dangling chains formed by cutting were also connected to the skeleton by residual crosslinkers and elongated by uniaxial swelling of the skeleton network. The cut surface is significantly rougher than the as-prepared surface (**Figure 4d**). In addition, it has a disordered network structure approximately 1 μm deep from the outermost surface, while the mesh structure is maintained in the inner region. The length of the created dangling chains at the cut surface is nearly equal to the bulk mesh size since these dangling chains originated from the mesh. Considering that cutting creates two fracture surfaces, the damage zone has a total depth of approximately 2 μm, suggesting that brittle hydrogel is fractured near the surface, despite the cut edge thickness of 76 μm. This observation provides molecular information about the relation between the microscale damage zone and macroscopic fracture.

2.4. Observation of large size heterogeneity

Characterization of large size heterogeneity and defects is vital in understanding the fracture of the material, as the latter is governed by local defects, not by the average structure[9,33]. Particularly, the fracture is always initiated from the largest defect in a material.

Here, we applied the developed method to directly observe the large-size defects in the hydrogel network.

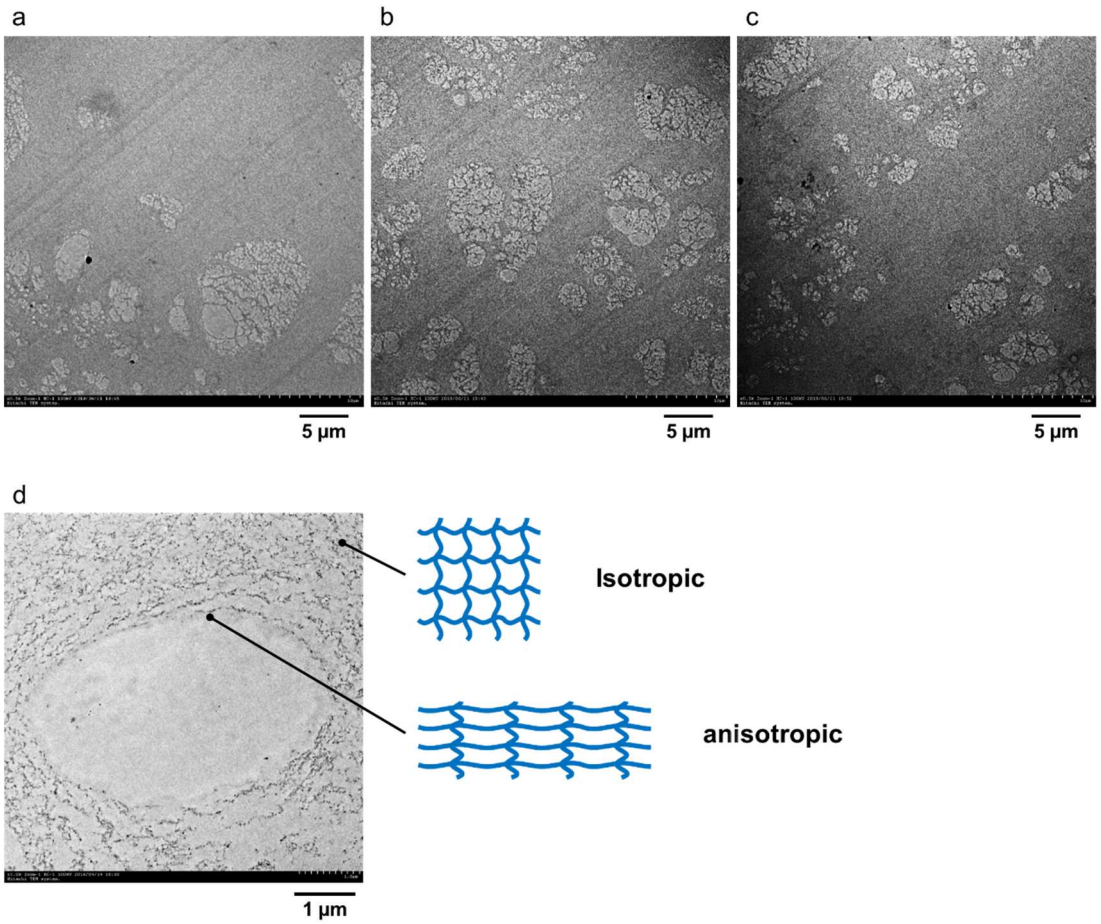

Figure 5. Micro-scale defects in the bulk PAMPS-4 gel. (**a**)–(**c**) Low magnification TEM images at different locations. The white areas reveal the presence of micro-voids with no PAMPS network. (**d**) High magnification TEM image around a micro-void and the polymer strands are aligned around the void as shown by the illustration.

Figure 5 shows the TEM images of a bulk PAMPS-4 hydrogel with the PDMAAm

362 skeleton network and its schematic illustrations. The PAMPS hydrogel contains many voids
363 of approximately 10 μm in diameter (**Figure 5a–c**). These micro-scale defects are not
364 observed in small microgels with a diameter of several micro-meters (**Figure S2**). TEM
365 observation allows simultaneous observation of the hydrogel structure at multiple scales.
366 **Figure 5d** shows a high magnification image of a void and its schematic illustrations.
367 Polymer strands around the void are oriented along the defect circumference, indicating that
368 these strands are highly elongated compared to those 2 μm away from the void surface. This
369 result denotes that microscale heterogeneity, such as void, induces nanoscale stress
370 concentration. Note that these micro voids are not always generated, depending on
371 polymerization kinetics and gel composition. The void formation has been predicted for the
372 hydrogels formed by free radical polymerization from monomer and crosslinker of the current
373 study [34,35]. During the polymerization, microgels are first formed, then these microgels grow
374 and coalesce to form bulk gels, resulting in voids in the unfilled space of microgels. Hence,
375 the TEM observation confirms that a microgel (**Figure S2**) is relatively homogeneous and
376 free of large defects, while bulk gels inevitably contain defects, thereby affecting their
377 mechanical properties.
378
379 **3. Conclusion**
380 We develop for the first time a method to image the hydrogel networks with nanoscale

resolution. This method allows us to directly observe the structure of the polyelectrolyte network from the nanoscale level to the microscale level. In this method, we selectively stain the target network at isovolumic conditions by mineralizing nanoparticles to achieve sufficient electron contrast and high spatial resolution. Although we only reported TEM imaging of hydrogels carrying negative charges, this method could be expanded to the hydrogels carrying positive charges using proper staining conditions. Moreover, it also could be applied to neutral polymers by appropriate chemical modification of side chains. For example, polyacrylamide hydrogel, one of the most common synthetic hydrogels, could be visualized by converting the amide side chain to carboxylic acid by hydrolysis.

The molecular structure of the network in bulk and on the surface was unveiled for the first time in real space. We clarified the presence of dangling chains on the surface of the as-prepared gels with a length scale the same as the mesh size. These results are essential in understanding the surface properties of hydrogels, including surface wetting–dewetting, sliding friction, adhesion, and bonding. Furthermore, numerous micro-scale defects are observed, around which polymer strands are aligned. These results are essential in understanding the origin of the brittleness of hydrogels. This direct imaging method provides rich information for understanding the underlying mechanism for many physical behaviors of the hydrogels from fracture to friction to adhesion.

4. Experimental Methods

Materials: The 2-acrylamido-2-methyl propanesulfonic acid (AMPS) monomer was provided by Toagosei Co. Ltd, Japan. The dimethylacrylamide (DMAAm) monomer, *N, N'*-methylenebisacrylamide (MBAA) crosslinker, 2-oxoglutaric acid (α-keto) initiator, iron (III) chloride hexahydrate and 2-morpholinoethanesulfonic acid monohydrate (MES) buffer were purchased from Wako Pure Chemical Ind., Ltd., Japan. Osmium tetroxide (OsO_4) was acquired from TAAB Laboratories Equipment Ltd., England. DMAAm monomer was purified by reduced pressure distillation before usage. The other chemicals were used as received.

Network sample synthesis: The PAMPS network was synthesized from precursor solution comprised of 1 M AMPS as the monomer, 1–8 mol% MBAA as the crosslinker, and 0.1 mol% α-keto as the initiator in water. Each mol% is relative to the corresponding monomer. The precursor solution was poured into a mould made of two glass plates separated with a 2 mm thick silicone spacer, and then was irradiated by UV for 8 h in a chamber filled with inert Ar gas. Then, the plate-shaped PAMPS gel was removed from the mould and immersed in water. The polyelectrolyte gel significantly swelled in water and the sample thickness swelling ratio λ_s in relative to its state at synthesis was 4.5 - 1.7 (**Supplementary Table S1**) for crosslinker ratio *Cx* of 1 - 8 mol%. The corresponding PAMPS polymer volume fraction was 0.2 – 3.8 vol.%. The samples were coded according to C_x as PAMPS-C_x.

To induce the skeleton network, the PAMPS gels removed from the mould were directly immersed in PDMAAm network precursor solution for 1 day until reaching equilibrium. The precursor solution of PDMAAm network was comprised of 2 M DMAAm monomer, 0.1 mol% MBAA, and 0.1 mol% α-keto in water. The PAMPS gel, substantially swelled in the PDMAAm network precursor solution, was sandwiched between two glass

plates and irradiated with UV for 6 h in Ar atmosphere to form PDMAAm skeleton network inside the target PAMPS network[21]. The obtained samples were immersed in distilled water for one week to completely remove residual chemicals. All glass plates used in the moulds were heated in a 500 ℃ oven for 1 h to remove any residual organics before use.

PAMPS-4 microgels and supermacroporous PAMPS-0.5 gel were also prepared by suspension polymerization and cryogelation, respectively, using the protocols reported.[26,27] The mesh size of the supermacroporous PAMPS-0.5 gel is less than that of conventional PAMPS-0.5 gel since the concentration of the precursor solution were increased by ice formation during freezing in the cryo-gelation. The PDMAAm network in these gels was introduced using the protocol described above.

Average mesh size estimation from bulk modulus: The average mesh sizes of the PAMPS network and the PDMAAm network was estimated from their bulk Young's modulus according to rubber elasticity theory. If we assume affine model, the Young's modulus E_0 of the network samples at the as-prepared state is related to the density of elastically effective strands v_0 as follows [28].

$$E_0=3v_0k_BT=3k_BT/\xi_0^3 \quad (1)$$

where k_B and T are Boltzmann constant and temperature, respectively, and ξ_0 is the mesh size at the as-prepared state. Here, it is assumed that each elastically active strand has energy of k_BT in the as-synthesized state. The average mesh sizes ξ of the PAMPS network and PDMAAm

network in TEM observation state were estimated from the thickness ratio λ_s of the resin-cured sample relative to their corresponding as-prepared states. Assuming the affine deformation, the polymer network mesh size was increased by a factor of λ_s in comparing with that in their as-prepared state.

$$\xi=\lambda_s\times\xi_0 \qquad (2)$$

The compressive stress-strain curves of the PAMPS single network gel and PDMAAm single network gel in their as-prepared state were measured using a mechanical tester (Tensilon RTC-1310A, Orientic Co., Japan). The samples were cut into discs with 15 mm diameter using a cutting machine. The test was performed at a strain rate of 1/600 s^{-1}. E_0 was estimated from the initial slopes of the stress-strain curves. Each test was performed on five samples.

Mineral staining: For mineral staining, the PAMPS hydrogels with PDMAAm skeleton were immersed in a staining aqueous solution of 2.5 M $FeCl_3$ for 1 day at 25 ℃. Subsequently, the gels were immersed in pure water or 0.1 M MES buffer solution at 25 ℃ to increase pH and amorphous ferric oxide (AFO) nanoparticles were mineralized on the PAMPS network. For TEM observation under vacuum condition, the water in the hydrogels must be removed without causing structure change of the target network. For this purpose, we adopted the established resin substitution process for preparing TEM specimen of biological tissues.[17] The mineralized hydrogels were immersed in ethanol to replace water with ethanol. The ethanol was then step wisely replaced by resin precursor of acrylic monomer liquid (London Resin white, medium),

462 and finally the samples were heated at 55 °C to obtain solidified resin in the chamber of an
463 automatic freeze substitution system (EM AFS2, Leica Microsystems, Germany). For all
464 PAMPS samples with different formulations, the final thickness changes of the resin-cured
465 specimen are within 10% relative to that of the PAMPS samples in water (**Figure 1c**, **Table S1**).
466 Then, 100 nm thick resin-cured specimens were cut using an ultra-microtome knife (EM UC7i,
467 Leica Microsystems, Germany) and then placed on a carbon-supported copper mesh grid for
468 TEM observation. We confirmed that the conventional electron stain (Osmium (VIII) oxide)
469 that labels one carbon–carbon double bond with one heavy atom could not provide enough
470 contrast to the sparse and extremely thin network of PAMPS hydrogels in TEM observation.
471 *Transmission electron microscopy (TEM) observation:* 2D TEM observations (H-7650,
472 Hitachi, Japan) were performed at an acceleration voltage of 100 kV of the electron gun. 3D
473 TEM[12,14] and energy dispersive X-ray spectrometry (EDS) were performed using a TEM
474 tomographic system (JEM-1400 and EM-05500TGP, JEOL, Japan) and a scanning transmission
475 electron microscope (STEM, JEM-F200, JEOL, Japan). The acceleration voltage of the electron
476 guns was 120 and 200 kV, respectively.
477 *TEM image analysis:* The total apparent polymer length in the 2D TEM images of PAMPS-
478 1 samples was estimated using ImageJ software[36] (**Figure S5**). The original TEM images were
479 binarized and then skeletonized and the total pixels were measured in the images of five
480 different places of the sample. Because TEM image shows projection of three-dimensional

481 object into two-dimensional plane, we corrected the 2D apparent polymer length to 3D length.
482 When a three-dimensional straight line is projected in 2D, the 2D apparent length is the original
483 length multiplied by cosθ, where θ is the angle of the line with respect to the projection plane.
484 In the view field, there are polymers with various directions, 0° to 180°. The integral value of
485 cosθ in the range of 0° to 180° is 2/π. Thus, 2D apparent polymer contour length in the viewed
486 field is related to the 3D length as,

487 $$L_{3D}=(\pi/2)L_{2D} \qquad (3)$$

488 *Estimation of theoretical contour length in TEM image:* The theoretical network strand
489 contour length L was calculated from the AMPS concentration $C = C_0/\lambda_s^3$ in the specimen after
490 resin exchange, where C_0 is the PAMPS monomer concentration at synthesis (The conversion
491 ratio of monomers in synthesis was close to 100%). The total contour length of PAMPS chain
492 in a TEM view volume V is

493 $$L= b\ C\ N_A V = bC_0 N_A V/\lambda_s^3 \qquad (4)$$

494 Here b is the monomeric length of PAMPS, and N_A is the Avogadro number. For PAMPS-1
495 sample, the swelling ratio from its as-prepared state λ_s=4.5 and b=0.25 nm. In this experiment,
496 the view field has a volume of V=896×896×100 nm^3 = 8.0×10^{-20} m^3. Thus, the theoretical
497 network strand contour length, including the loops and dangling chains, is estimated as L=1.3
498 ×10^5 nm.

499 *A simple model to estimate contour length from cut-off length of stained polymer:* Since

500 the polymer strands could collapse at a length scale smaller than the cut-off length ξ_c by mineral
501 staining, we need make a correction of this effect to estimate the total true contour length from
502 the total apparent chain length obtained from TEM images. Denoting N_{sub} as the Kuhn monomer
503 number of a subsection of the strand with the end-to-end distance ξ_{sub} equal to cut-off length ξ_c
504 ($\xi_{sub}=\xi_c$) before staining, the contour length of such subsection of strand $L_{sub}=b_K N_{sub}$, where b_K
505 is Kuhn length of the polymer at the as-prepared state. On the other hand, the corresponding
506 end-to-end distance of the subsection strand at the as-prepared state $\xi_{sub0} = \xi_{sub}/\lambda s$ assuming
507 affine deformation by swelling. Since water is good solvent for PAMPS (χ =0.30-0.35)[37],
508 $\xi_{sub0}= b_K N_{sub}^{3/5}$. Hence, the fraction of shrinkage

509 $$L_{sub}/\xi_{sub}= (\xi_c/\lambda s b_K)^{2/3}/\lambda s \quad (5)$$

510 Using λs=4.5, $\xi_{sub}=\xi_c$ =40 nm, and b_K=0.5 nm[38], we have L_{sub}/ξ_{sub}=1.4 for PAMPS-1 sample.
511 Therefore, a correct factor of 1.4 should be considered to get the true contour length from the
512 stained contour length of TEM.
513

514 **Supporting Information**

515 Supporting Information is available from the Wiley Online Library or from the author.
516

517 **Acknowledgements**

518 R.K., T.N. and J.P.G. perceived the concept, designed the experiments and interpreted the

results. R.K. performed most experiments and analysed the data. M.Y. performed TEM observation for the gels with different crosslinker ratios. T.S. prepared the porous gel. H.J. performed STEM measurements. All the authors participated the discussion. R.K., T.N. and J.P.G. wrote the paper. J. P. G. thanks the JSPS KAKENHI (No. JP17H06144, JP17H06376, JP22H04968), R.K. thanks the JSPS Research Fellow (No. JP16J05057) and the Ambitious Leaders Program. H. J. is grateful to the JSPS KAKENHI for the partial support of this research through Grant No. 19H00905 and 22H00329. R. K. thanks Kazuki Fukao, Takahiro Matsuda, and Taiki Fukuda (Hokkaido University) for their useful comments. The authors also thank Takeshi Higuchi (Tohoku University), Haruka Ai and Yoshitaka Aoyama (JEOL, Japan) for their kind help with the STEM measurements. The authors thank the late Dr. Daniel R. King for his helpful comments.

References

[1] A. S. Hoffman, *Adv. Drug Deliv. Rev.* **2012**, *64*, 18.

[2] O. Erol, A. Pantula, W. Liu, D. H. Gracias, *Adv. Mater. Technol.* **2019**, *4*, 1900043.

[3] R. A. Green, S. Baek, L. A. Poole-Warren, P. J. Martens, *Sci. Technol. Adv. Mater.* **2010**, *11*, 014107.

[4] T. Sekitani, T. Yokota, K. Kuribara, M. Kaltenbrunner, T. Fukushima, Y. Inoue, M. Sekino, T. Isoyama, Y. Abe, H. Onodera, T. Someya, *Nat. Commun.* **2016**, *7*, 11425.

[5] J. Bastide, L. Leibler, *Macromolecules* **1988**, *21*, 2647.

[6] M. Shibayama, T. Norisuye, *Bull. Chem. Soc. Jpn.* **2002**, *75*, 641.

[7] M. Shibayama, *Macromol. Chem. Phys.* **1998**, *199*, 1.

[8] H. Tsukeshiba, M. Huang, Y.-H. Na, T. Kurokawa, R. Kuwabara, Y. Tanaka, H. Furukawa, Y. Osada, J. P. Gong, *J. Phys. Chem. B* **2005**, *109*, 16304.

[9] A. A. Griffits, *Philos. Trans. R. Soc. London. Ser. A, Contain. Pap. a Math. or Phys. Character* **1921**, *221*, 163.

[10] M. Rubinstein, R. H. Colby, *Polymer Physics*, Oxford Univ. Press, Oxford, **2003**.

[11] H. Furukawa, K. Horie, *Phys. Rev. E* **2003**, *68*, 1.

[12] H. Jinnai, R. J. Spontak, T. Nishi, *Macromolecules* **2010**, *43*, 1675.

[13] R. Vitali, E. Montani, *Polymer (Guildf).* **1980**, *21*, 1220.

[14] H. Jinnai, T. Higuchi, X. Zhuge, A. Kumamoto, K. J. Batenburg, Y. Ikuhara, *Acc. Chem. Res.* **2017**, *50*, 1293.

[15] R. Aso, H. Kurata, T. Namikoshi, T. Hashimoto, S. Kuo, F. Chang, H. Hasegawa, M. Tsujimoto, M. Takano, S. Isoda, *Macromolecules* **2013**, *46*, 8589.

[16] M. Tosaka, R. Danev, K. Nagayama, *Macromolecules* **2005**, *38*, 7884.

[17] G. R. Newman, B. Jasani, E. D. Williams, *Histochem. J.* **1983**, *15*, 543.

[18] N. A. Ranson, P. G. Stockley, in *Emerg. Top. Phys. Virol.*, IMPERIAL COLLEGE PRESS, **2010**, pp. 1–33.

[19] S. Onogi, H. Shigemitsu, T. Yoshii, T. Tanida, M. Ikeda, R. Kubota, I. Hamachi, *Nat. Chem.* **2016**, *8*, 743.

[20] F. Gentile, M. Moretti, T. Limongi, A. Falqui, G. Bertoni, A. Scarpellini, S. Santoriello, L. Maragliano, R. Proietti Zaccaria, E. di Fabrizio, *Nano Lett.* **2012**, *12*, 6453.

[21] J. P. Gong, Y. Katsuyama, T. Kurokawa, Y. Osada, *Adv. Mater.* **2003**, *15*, 1155.

[22] J. P. Gong, *Soft Matter* **2010**, *6*, 2583.

[23] K. Yasuda, N. Kitamura, J. P. Gong, K. Arakaki, H. J. Kwon, S. Onodera, Y. M. Chen, T. Kurokawa, F. Kanaya, Y. Ohmiya, Y. Osada, *Macromol. Biosci.* **2009**, *9*, 307.

[24] T. Nakajima, T. Chida, K. Mito, T. Kurokawa, J. P. Gong, *Soft Matter* **2020**, *16*, 5487.

[25] C. M. Flynn, *Chem. Rev.* **1984**, *84*, 31.

[26] J. Hu, K. Hiwatashi, T. Kurokawa, S. M. Liang, Z. L. Wu, J. P. Gong, *Macromolecules* **2011**, *44*, 7775.

[27] T. Sedlačík, T. Nonoyama, H. Guo, R. Kiyama, T. Nakajima, Y. Takeda, T. Kurokawa, J. P. Gong, *Chem. Mater.* **2020**, *32*, 8576.

[28] K. Fukao, T. Nakajima, T. Nonoyama, T. Kurokawa, T. Kawai, J. P. Gong, *Macromolecules* **2020**, *53*, 1154.

[29] J. Katta, Z. Jin, E. Ingham, J. Fisher, *Med. Eng. Phys.* **2008**, *30*, 1349.

[30] A. Jackson, W. Gu, *Curr. Rheumatol. Rev.* **2009**, *5*, 40.

[31] T. Nakajima, H. Furukawa, Y. Tanaka, T. Kurokawa, Y. Osada, J. P. Gong, *Macromolecules* **2009**, *42*, 2184.

[32] M. Frauenlob, D. R. King, H. Guo, S. Ishihara, M. Tsuda, T. Kurokawa, H. Haga, S. Tanaka, J. P. Gong, *Macromolecules* **2019**, *52*, 6704.

[33] M. Marder, J. Fineberg, *Phys. Today* **1996**, 24.

[34] S. Seiffert, *Polym. Chem.* **2017**, *8*, 4472.

[35] N. Ide, T. Fukuda, *Macromolecules* **1999**, *32*, 95.

[36] C. A. Schneider, W. S. Rasband, K. W. Eliceiri, *Nat. Methods* **2012**, *9*, 671.

[37] T. Tominaga, V. R. Tirumala, S. Lee, E. K. Lin, J. P. Gong, W. Wu, *J. Phys. Chem. B* **2008**, *112*, 3903.

[38] S. Cui, C. Liu, Z. Wang, X. Zhang, S. Strandman, H. Tenhu, *Macromolecules* **2004**, *37*, 946.

Table of Content

Direct observation of the nanoscale polymer network of hydrogels is essential in understanding its properties. Herein, for the first time, we developed a novel staining and structure fixation method for TEM observation to visualize the hydrogel network architecture in its unperturbed conformation with nanometer resolution. The revealed molecular structures on surface and bulk hydrogels provide important insights for the friction, adhesion, and fracture of hydrogels.

Ryuji Kiyama, Masahiro Yoshida, Takayuki Nonoyama, Tomáš Sedlačík, Hiroshi Jinnai, Takayuki Kurokawa, Tasuku Nakajima, and Jian Ping Gong**

Nanoscale TEM Imaging of Hydrogel Network Architecture